INTERNATIONAL ATOMIC ENERGY AGENCY
UNITED NATIONS EDUCATIONAL, SCIENTIFIC AND CULTURAL ORGANIZATION
INTERNATIONAL CENTRE FOR THEORETICAL PHYSICS
I.C.T.P., P.O. BOX 586, 34100 TRIESTE, ITALY, CABLE CENTRATOM TRIESTE

H4.SMR/453-45

TRAINING COLLEGE ON PHYSICS AND CHARACTERIZATION OF LASERS AND OPTICAL FIBRES

(5 February - 2 March 1990)

GAS AND MOLECULAR LASERS

Prof. S. Solimeno
&
Prof. A. Cutolo

Università di Napoli

NOTES ON GAS AND MOLECULAR LASERS

Salvatore Solimeno
Dip. Scienze Fisiche
Mostra d'Oltremare Pad.16
80125 NAPOLI

Antonello Cutolo
Dip.Ing.Elettronica
Via Claudio 21
80125 NAPOLI

Contents

BASIC THEORY ON GAS AND MOLECULAR LASERS

WAVEGUIDE GAS LASERS

BASIC THEORY ON GAS AND MOLECULAR LASERS

1. Internal_Energy_Levels_in_Gases

Atomic species possess only translational and electronic energy. For diatomic molecular species, the energy level structure is of course more complex because of the appearance of rotational and vibrational states. These can overlap each other, as illustrated in Figure , in which v represents the vibrational level number and J the rotational level number. For a rigid rotator, the rotational energy per molecule is

$$E_{rot}(J) = hc\, B_e\, J(J+1) \qquad (1)$$

where $B_e = h/8\pi^2 I$ is the rotational constant in cm^{-1}, and I is the moment of inertia of the molecule. The level spacing increases with J. In particular, $B_e \approx 4\ cm^{-1}$ for CO_2 and 1.9 cm^{-1} for CO.The vibrational energy for a harmonic oscillation is

$$E_{vib}(v) = hc\, w_e\, (v + ½) \qquad (2)$$

per molecule, where $w_e = \omega_{vib}/c$ is the wave number in cm^{-1}, giving equally spaced energy levels. However, anharmonic effects become important at large values of v. A similar vibrational-rotational structure is repeated in electronically excited states.

In particular a diatomic molecule can be represented as a Morse vibrator characterized by the potential

$$v(r) = D_o \left\{1 - \exp[-\beta(r-r_e)]\right\}^2$$

where D_o represents the dissociation energy and r_e the equilibrium internuclear distance. The vibrational wavefunction is given by

$$\Psi_v(x) \propto e^{-z/2}\, z^{(k-1)^{-n/2}}\, L_{k-v-1}^{k-2v-1}(z)$$

where $k=4D_o/h\omega_e$ and $z=k\exp(-\beta r_e x)$, $x=r/r_e$. L_α^γ represents the Laguerre polynomial.

In addition, the roto-vibrational energy reads

$$\frac{E_{vj}}{hc} = \omega_e\left(v + \frac{1}{2}\right) - \omega_e x_e \left(v + \frac{1}{2}\right)^2 + B_e J(J+1) - \alpha_e\left(v + \frac{1}{2}\right) J(J+1)$$

$$- D_e J^2 (J+1)^2 \ (cm^{-1})$$

The triatomic molecule CO_2 has the following vibrational degrees of freedom: symmetrical stretching (v_1) degenerate bending (v_2) and asymmetric stretching (v_3). Their vibrational levels are numbered

$$\begin{array}{ll} v_1 & 000,\ 100,\ 200\ \ldots \\ v_2 & 000,\ 010,\ 020\ \ldots \\ v_3 & 000,\ 001,\ 002\ \ldots \end{array} \qquad (3)$$

where 000 denotes the vibrational ground state. Each of these modes has its own ladder of quantized energy levels, with the triple-quantum number notation (v_1, v_2, v_3) to designate each level. CO_2 is the lasing molecule, and of particular importance is the (001) upper_laser_level in the v_3 mode, and the (100) lower laser level in the v_1 mode. This laser transition takes place at a wavelength depending on the particular rotational levels involved. In fact, note that each vibrational level has a series of closely spaced rotational levels superimposed on it, and the actual laser transition takes place between two distinct vibration-rotation levels. These levels are shown schematically in Figure , where J denotes the rotational quantum number. A radiative transition that results in $\Delta J=-1$ is a member of the "P Branch", If the gas transitional temperature is near room temperature, and the laser cavity is properly tuned, the P(20) transition is generally observed.

The bending mode is doubly degenerate and the relative wavefunction is represented by

$$\Psi_{ve} \propto \exp\left(-\frac{\alpha\rho^2}{2}\right) P_v^{\ell}(\alpha^{1/2}\rho)\exp(\pm il\varphi)$$

where $\rho^2=x^2+y^2$, $\varphi=\arctan y/x$ and P_v^{ℓ}. The index ℓ can take the values $v_1 v_2 \ldots$ 1 or 0 only. Accordingly, 1 represents a rotational quantum number associated with the bending mode to $1=0,1,2,3$ ... correspond the species Σ, Γ, Δ, Φ etc. Each vibrational level is v+1 times degenerate. In particular,

v	1	species
0	0	Σ
1	1	Γ
2	2,0	Δ, Σ
3	3,1	Φ, Γ

The levels $100(\Sigma_g^+)$ and $020(\Sigma_g^+, \Delta_g)$ exhibit an accidental degeneracy (Fermi resonance). Conseguently, the levels $02^00(\Sigma_g^+)$ and $02^20(\Delta_g)$ become split apart 100 cm^{-1}.

2. Collisional Excitation Processes

Consider an inelastic, binary collision process such as

$$A + B \rightarrow C + D \qquad (4)$$

where A, B, C, D may be either different energy states of the same molecule, or different species. Let R_{AB} be the thermally averaged rate of formation of C and D from A and B, per unit volume and time. Assuming a Maxwellian velocity distribution, the number of collisions per unit volume and time between A and B molecules is

$$Z_{AB} = \sigma_{AB}\sqrt{\frac{8\ kT}{\pi\ \mu_{AB}}}\ N_A\ N_B \qquad (5)$$

where N_A and N_B are the numbers of molecules per unit volume

$$\mu_{AB} = \frac{m_A\ m_B}{m_A + m_B} \qquad (6)$$

is the reduced mass, and σ_{AB} is the collision cross-section for A+B collisions. The rate R_{AB} of the inelastic collision process may be expressed in terms of an inelastic cross section, σ_{AB}

$$R_{AB} = \sigma_{AB}\sqrt{\frac{8\ kT}{\pi\ \mu_{AB}}}\ N_A\ N_B$$

σ_{AB} may be functions of the temperature T or, in the absence of internal energy equilibrium, of the distribution of internal energy.

A brief review follows of some of the types of inelastic collisional processes involved in the formation and depletion of population inversions in gas lasers.

(i) Electron impact (collision of the first kind)

$$A + (e + KE) - A^* + e \qquad (\quad)$$

where KE denotes the kinetic energy of the incident electron, and A^* is an excited state of A. An example from the helium-neon laser is

$$N_e + (e + KE) \rightarrow N_e\ (2s_4) + e \qquad (\ )$$

(ii) Atom-atom collisions (collisions of second kind)

$$A + B^* \rightarrow A^* + B \pm \Delta E \qquad (\ )$$

Generally, the maximum cross sections are appreciably greater than 10^{-16} cm^2 only for optically allowed transitions in both atoms. An example of an atom-atom collision process is

$$H_e{}^*(2^3\ S_1) + N_e - N_e\ (2S_{3,4,5}) + H_e + \Delta E$$

(iii) Atom-molecule collisions

Several different types of process may be considered under this heading. The first is dissociation excitation

$$A^* + BC \rightarrow A + B^* + C^* \pm \Delta E \qquad (13)$$

where B and C may or may not end up in excited states simultaneously. The probability for processes of this type is greatest if the energy discrepancy E is small, but this requirement is not as stringent as in the atom-atom exchange process (3.11). Another type of process is the atom exchange reaction

$$A + BC \rightarrow AB^* + C$$

and example of which is

$$F + H_2 \rightarrow HF^* + H$$

in which HF is formed in a vibrationally excited state.

(IV) Molecule-molecule collisions

Vibrational energy exchange is an important case to be considered under this heading. The probability per collision of vibration-translation exchange is generally very small, and excitation and de-excitation occur mainly in single-quantum jumps, e.g.

$$N_2(v) + M \rightarrow N_2(v + 1) + M$$

The probability increases only linearly with v, but exponentially with temperature, the temperature dependence being approximately as

$$\exp\left[-\left(\frac{8\pi^2\ v^2\ L^2\ \mu}{kT}\right)^{1/3}\right]$$

where L is a range parameter and μ is the reduced mass of the collision. Vibration-vibration exchange has a relatively high probability per collision for a resonant or near-resonant exchange, but the probability drops sharply, to values comparable to those for vibration-translation exchange, as the energy mismatch approaches kT. Thus for example in the process

$$N_2(v') + N_2(v'') - N_2(v' + 1) + N_2(v'' - 1)$$

the probability per collision is high in the near-resonant process if $v' \approx v''$. Similarly

$$N_2(v = 1) + CO_2(000) \rightarrow N_2(v = 0) + CO_2(001) - 18\ cm^{-1}$$

has much greater probability than

$$N_2(v = 1) + CO_2(000) - N_2(v = 0) + CO_2(100) + 900\ cm^{-1}$$

In many situations it is sufficient to assume a Maxwell-Boltzmann distribution among rotational levels. Since each rotational level with quantum number J has a (2J + 1)-fold degeneracy, which appears as a multiplying factor, the expression for equilibrium is

$$N_J = N_v\,(2J+1)\left[\frac{\exp\left(-E_{rot}(J)/kT\right)}{\sum_{J=1}^{\infty}(2J+1)\exp\left(-E_{rot}(J)/kT\right)}\right]$$

where N_J is the population density of rotational level J of vibrational level v.

3. Gain

For a molecular transition, the gain expression must take account the large number of rotational levels in a given vibrational level. So colled P-branch transitions (v → v -1, J → J + 1) must be treated separately from R-branch transitions (v → v - 1, J → J - 1).

The small signal gain is

$$\alpha_{vj}^{v'j'} = \frac{K}{2} B_{vj}^{v'j'} \nu_o\, g(\nu_o)\,\Delta N$$

where ν_o is the laser frequency, g(v) the line profile, $B_{vj}^{v'j'}$ the Einstain coefficient and ΔN the population inversion. For a laser operating on a P-branch,

$$\Delta N = N_V \frac{N_j}{N_v} - \frac{g_j}{g_{j+1}} N_{v'} \frac{N_{j+1}}{N_{v'}}$$

with $g_j = 2j+1$ the degeneracy factor. Relying on the expression of N_j we have

$$N = N_v \frac{N_J}{N_v}\left[1 - \frac{N_{v'}}{N_v}\exp\left(-\frac{2B}{kTrot}(J+1)\right)\right]$$

It is worth noting that ΔN>0 also for $N_{v'} < N_{v'}$ if we consider rotational numbers sufficiently high (partial inversion)(see figure obtained by Patel for CO),

$$J > \frac{kT_{rot}}{2B} \ln \frac{N_v}{N_{v'}}$$

For a CO_2 the laser transition exhibits a collisional broadening, so that

$$g(v) = \frac{1}{2\pi}\,\frac{v}{(v-v_o)^2+(v/2)^2}$$

In particular, $\Delta\nu \sim 4$GHz at STP.

The Einstein coefficient B is given by

$$B_{vj}^{v'j'} = \frac{(2\pi)^4}{3h^2 c g_{vj}} \sum_{J_2 J'_2} \left|p_{vJ\,x}^{v'j'}\right|^2$$

$$= (2\pi)^2 \cdot 10^{57}\,\frac{J'+J+1}{2J+1}\,\left|p_{vj}^{v'j'}\right|^2$$

being $p_{vj}^{v'j'}$ the dipole moment matrix element for an electric field supposed polarized along the x-axis

$$p_{vj}^{v'j'} = e\int \Psi^{*}_{v'j'}(r_n)\,\Psi_{vj}(r_n)\,d^3 r_n \cdot \int \Psi_e^{*}(r_e r_n)\,x_e\,\Psi_e(r_e r_n)\,d^3 r_e$$

where $\vec{r}_e$ and $\vec{r}_n$ refer to the electrons and nuclei respectively. Ψ_e is the electron wavefunction relative to an assigned position of the nuclei.

Setting

$$\mu(r_n) = e \int \Psi_e^*(r_e r_n) x_e \Psi_e(r_e r_n)\, d^3 r_e$$

$$= M_o + M_1 |\vec{r}_A - \vec{r}_o| + M_2 |\vec{r}_A - \vec{r}_o|^2 + \ldots$$

with r_o the equilibrium value of r_n, we have

$$P_{vj}^{v'j'} = \int \Psi_{v'j'}^*(r_n)\, \mu(r_n)\, \Psi_{vj}(r_n)\, d^3 r_n$$

In particular for the HF molecule

$$\langle 0 |\mu| 0 \rangle = 1.819 \cdot 10^{-10} \text{ esu} \cdot \text{cm}$$
$$\langle 1 |\mu| 0 \rangle = 9.85 \cdot 10^{-20} \text{ esu} \cdot \text{cm}$$
$$\langle 2 |\mu| 0 \rangle = 1.25 \cdot 10^{-20} \text{ esu} \cdot \text{cm}$$
$$\langle 3 |\mu| 0 \rangle = 1.63 \cdot 10^{-21} \text{ esu} \cdot \text{cm}$$

$$\mu(r) = 1.78 + 1.52 \cdot (r - r_e) - 0.23 \cdot (r - r_e)^2 + \ldots$$

and the Einstain coefficient A are equal to

$A(1,0) = 189 \text{ sec}^{-1}$

$A(2,1) = 322 \text{ sec}^{-1}$

$A(3,2) = 406 \text{ sec}^{-1}$

$A(4,3) = 446 \text{ sec}^{-1}$

Patel has derived general expressions for the gain on vibrational-rotational transitions of a molecular laser, assuming:

(a) rotational thermalization very fast in comparison with vibrational relaxation, so that the rotational level population can be described by a Boltzmann distribution at a characteristic temperature T_{rot};

(b) temperatures, T_{rot}, are the same for upper and lower vibrational levels;

(c) only vibrational rotational transitions are considered, so only P and R branches are allowed.

The gain expression is

$$\alpha_{vJv'J'} = \frac{8\pi^3 c^4 K_{vv'} S_J Z_{vJv'J'}}{3kT_{rot} (2\pi kT/m)^{1/2}}$$

$$\left[N_v B_v \exp\left(-F_v(J) \frac{hc}{kT_{rot}}\right) - N_{v'} B_{v'} \exp\left(-F_{v'}(J') \frac{hc}{kT_{rot}}\right) \right]$$

where

$\alpha_{vJv'J'}$ = optical gain per unit length at centre of $J - J'$, $v - v'$ transition

$K_{vv'} S_J Z_{vJv'J'} = |R_{vJv'J'}|^2$ = matrix element for transition

$K_{vv'}$ = vibrational contribution to matrix element

$S_J Z_{vJv'J'}$ = rotational contribution to matrix element

S_J = J + 1 for P-branch; J for R-branch

$Z_{vJv'J'}$ = vibration-rotation interaction factor for transition (unity for rigid rotor)

m = molecular mass

N_v, $N_{v'}$ = total population densities in v and v' vibrational levels, respectively

B_v, $B_{v'}$ = rotational constants for levels v and v' respectively

F(J) = energy of Jth rotational from 0th level

$$= BJ(J + 1) - DJ^2(J + 1)^2 \text{ with } D \ll J.$$

This equation has been used to calculate the gain for CO with $T_{rot} = T$, as a function of the various parameters. The gain $\alpha_{vJv'J'}$ has been normalized by dividing by

$$\frac{8\pi^3 c^4 K_{vv'}}{3k\,(2\pi k/m)^{1/2}} N_{v'}$$

Vibrational Model

Figure 10 shows a schematic diagram of the major partecipartting vibrational energy levels for CO_2 and N_2. In 1969, Taylor and Bitterman made a thorough study and compilation of the collisional transition probabilities for CO_2-N_2 system. Their results show an extremely fast, resonant, vibrational energy exchange between v = 1 level of N_2 and the (001) level of CO_2, as well as a very fast exchange between the (100) and (020) levels of CO_2 due to Fermi resonance. In addition, vibrational energy is rapidly transferred among the lower excited levels of the degenerate mode v_2 in CO_2 due to the nearly equal spacing of these levels. Hence, these fast transitions appear to justify a vibrational model which groups the partecipating levels into two "modes" which are assumed in equilibrium within themselves, but not with each other.

In the following discussion of the vibrational model, a CO_2 N_2 mixture will be assumed.

The net vibrational energies per unit mass contained within each "mode", $(e_{vib})_I$ and $(e_{vib})_{II}$, are chosen as the dependent non-equilibrium variables. The relaxation of these energies is assumed to be described by

the simple-harmonic oscillator relaxation equations:

$$\dot{w}_2 = \frac{d(e_{vib})_I}{dt} = \frac{1}{\tau_I}\,[(e_{vib})_I^{eq} - (e_{vib})_I]$$

when $q_i = (e_{vib})_I$, and

$$\dot{w}_1 = \frac{d(e_{vib})_{II}}{dt} = \frac{1}{\tau_I}\, e_{vib}\,{}_{II}^{eq} - (e_{vib})_{II}$$

when $q_i = (e_{vib})_{II}$. $(e_{vib})_I^{eq}$ and $(e_{vib})_{II}^{eq}$ are the equilibrium vibrational energies that would be contained in Modes I and II respectively at the local gas translational temperature T, and τ_I and τ_{II} are the characteristic relaxation times for Modes I and II respectively. τ_I and τ_{II} are averages which characterize the net rate of energy transfer into and out of Modes I and II; this energy transfer is assumed to be governed by the major transitions which are identified with the relaxation times τ_a, τ_b, τ_c. These relaxation times are themselves averages of the detailed CO_2-CO_2, CO_2-N_2, CO_2H_2O, N_2-N_2 and N_2-H_2O collisions;

$$\frac{1}{\tau_a} = \frac{X_{CO_2}}{\tau_a(CO_2\text{-}CO_2)} + \frac{X_{N_2}}{\tau_a(CO_2\text{-}N_2)} + \frac{X_{He}}{\tau_a(CO_2\text{-}He)}$$

$$\frac{1}{\tau_b} = \frac{X_{CO_2}}{\tau_a(N_2\text{-}CO_2)} + \frac{X_{N_2}}{\tau_b(N_2\text{-}N_2)} + \frac{X_{He}}{\tau_b(N_2\text{-}He)}$$

$$\frac{1}{\tau_c} = \frac{X_{CO_2}}{\tau_c(CO_2\text{-}CO_2)} + \frac{X_{N_2}}{\tau_c(CO_2\text{-}N_2)} + \frac{X_{He}}{\tau_c(CO_2\text{-}He)}$$

x_i denotes the mole fraction of chemical species i. In turn, the average relaxation times for Modes I and II are obtained from

$$\tau_I = \tau_c$$

$$\frac{1}{\tau_{II}} = \left[\frac{X_{CO_2}}{\tau_a} + \frac{X_{N_2}}{\tau_b} \right] \cdot \frac{1}{(X_{CO_2} + X_{N_2})}$$

The quantity τ can be interpreted as a mean time required for a single particle to make a transition from one state to another

from one state to another state due to collisions with other particles. In turn, τ^{-1} can be interpreted as the number of transitions per second per particle. Hence, on a physical basis, the above equations simply state that the total number of transitions per second per particle due to collisions with all species present in the mixture is the sum of the transitions per second per particle due to collisions with each individual species.

It is sufficient to state here that the model is intended only for the calculation of population inversions in CO_2-N_2-He mixtures; it is not necessarily valid for other gases, nor can it be used when substantial amounts of radiative energy interact with the gas.

Returning again to the above equations $(e_{vib})_I$ and $(e_{vib})_{II}$ are used as the dependent nonequilibrium variables. From these energies, different vibrational temperatures $(T_{vib})_I$ and $(T_{vib})_{II}$, are obtained from the following equilibrium relations:

$$(e_{vib})_I = cCO_2\ RCO_2\ \left(\frac{h\nu_1}{k}\right)\ [e^{h\nu_1/kT_{vibI}}-1]^{-1} + (2h\nu_2/k)\ [e^{h\nu_2/kT_{vibI}}-1]^{-1}$$

and

$$(e_{vib})_{II} = cCO_2\ RCO_2\ \left(\frac{h\nu_3}{k}\right)\ [e^{h\nu_3/kT_{vibII}}-1]^{-1} + cN_2\ RN_2\ \left(\frac{h\nu}{k}\right)\ [e^{h\nu/kT_{vibII}}-1]^{-1}$$

cCO_2 and RCO_2 are the mass fraction and specific gas constant respectively for CO_2; cN_2 and RN_2 are defined similarly for N_2; ν_1, ν_2 and ν_3 are the normal vibrational frequencies of the symmetric stretching, the bending and the asymmetric stretching modes respectively for CO_2; and ν is the normal vibrational frequency for N_2. In turn, $(T_{vib})_I$ and $(T_{vib})_{II}$ are used to compute populations of energy levels within Modes I and II assuming a Boltzmann distribution locally within each mode. For example, the population of the (001) level in CO_2 is obtained from

$$N_{001} = NCO_2\ \ e^{-h\nu_3/kT_{vibII}}/Q$$

where

$$Q = [1 - e^{-h\nu_1/kT_{vibI}}]^{-1}\ [1 - e^{-h\nu_2/kT_{vibI}}]^{-2}\ [1 - e^{-h\nu_3/kT_{vibII}}]^{-1}$$

and the population of the (100) level in CO_2 is obtained from

$$N_{100} = NCO_2\ \ e^{-h\nu_1/kT_{vibI}}/Q$$

As a final note with regard to the present analysis, $(e_{vib})_I$ and $(e_{vib})_{II}$ are inherent parts of the time-dependent nonequilibrium nozzle flow solution, and are computed at each time step during the transient approach to steady-state conditions. Then, after the steady-state is achieved, the vibrational temperatures and populations are computed.

5. Electric molecular laser discharges

Electron kinetic processes in CO_2 and CO lasers discharge are difficult to analyze because of the numerous vibrational and electronic excitation processes of importance in molecular gases. Calculation of excitation rates is complicated by the fact that the electron energy distribution are non-Maxwellian in most conditions typical of CO_2 laser operation. W.L. Nighan and J.J. Lowke have made calculations of the distribution function, the fractional power transfer and the vibrational excitation rates in gas mixtures for several ratios CO_2:N_2:He. Using these calculated electron molecule rate constant along with those for molecule-molecule energy relaxation, it is possible to develop a model of CO_2 or CO molecular kinetics processes to predict the laser performance.

A/ - Electron energy distribution

The electron energy distribution function is obtained by solving the Boltzmann-Fokker-Planck equation in the form appropriated to the behaviour of low and moderate energy electron in a uniform d.c. electric field.

$$\frac{\partial f}{\partial t} + \vec{v} \cdot \nabla f - \frac{e}{m} \vec{E} \cdot \nabla_v f = \left(\frac{\partial f}{\partial t}\right)_c$$

where $f(v,\vec{r},t)$ is the electron velocity-position distribution and the right side represents the rate of change of f due to collisions. For a uniform gas we can drop the term proportional to $\vec{v}$. In addition, we can assume a near-isotropic distribution,

$$f(\vec{v}) = f_0(v) + \hat{v} \cdot \vec{f}_1(v)$$

Plugging this decomposition into the Boltzmann equation yields

$$\begin{aligned}\frac{\partial \vec{f}_1}{\partial t} - \frac{e}{m} \vec{E} \frac{\partial f_0}{\partial v} &= \left(\frac{\delta \vec{f}_1}{\delta t}\right)_c \\ \frac{\partial f_0}{\partial t} - \frac{e}{3mv^2} \vec{E} \cdot \frac{\partial}{\partial v}(v^2 \vec{f}_1) &= \left(\frac{\delta f_0}{\delta t}\right)_c\end{aligned}$$

Considering elastic collisions only we have

$$\left(\frac{\delta \vec{f}_1}{\delta t}\right)_c = -NQ_m(v) v \vec{f}_1(v)$$

Q_m being the momentum-transfer cross section. Since $NQ_m v$ is of the order of few picoseconds in a CO_2 laser we have

$$\vec{f}_1 = \frac{e}{m} \frac{1}{NQ_m v} \frac{\partial f_0}{\partial v} \vec{E}$$

Eliminating $\vec{f}_1$ and making a change in the independent variable

$$u = \frac{mv^2}{2e} \quad (volts)$$

we obtain the Boltzmann equation written in the form used by Frost and Phelps

$$\frac{\partial f_0}{\partial t} = 2 \frac{e}{m} \frac{1}{v} \frac{\partial}{\partial u} \left[\frac{uE^2}{3NQ_m} \frac{\partial f_0}{\partial u} + 2 \frac{m}{M} NQ_m u^2 \left(f_0 + KT \frac{\partial f_0}{\partial u} \right) \right]$$

$$\left(\frac{\delta f_0}{\delta t}\right)_c$$

$$\left(\frac{\delta f_0}{\delta t}\right)_c = \frac{2e}{mv} \times \sum_j \{[(u+u_j)f_0(u+u_j)N_0Q_j(u+u_j) - uf_0(u)N_0Q_j(u)]$$
$$+ [(u-u_j)f_0(u-u_j)N_jQ_{-j}(u+u_j) - uf_0(u)N_jQ_{-j}(u)]\}$$

Q_j represents the inelastic cross-section related to the j-th excitation process in which the energy u_j is transferred from the electron to the molecule. Q_{-j} is related to the inverse process in which the energy is transferred from the molecule to the electron, and is related to Q_j through detailed balance,

$$Q_{-j}(u) = \frac{u+u_j}{u} Q_j(u+u_j)$$

The Boltzmann equation can be written in a simplified form by retaining the most important terms only.

$$-\frac{(E/N)^2}{3}\frac{d}{du}\left(\frac{u}{Qm}\frac{df}{du}\right) = \sum_{D_R}[(u+u_j) \cdot f(u+u_j) \cdot QD_R(u+u_j) - u\,f(u)\,Q(u)]$$

Here f is the isotropic part of the distribution function, N is the neutral density, e and m are the electrical charge and mass, respectively, k is the Boltzmann constants, and u is the electron energy in volts. The elastic cross section is Q_m and Q_j is the inelastic cross section for the j th inelastic process.

The LHS of last equation accounts for the gain in energy due to the electric field E, the first term on the RHS involving a summation accounts for electrons of energy u + u_j losing energy u_j. Integrating and dividing by N, the following first-order integro differential equation results:

$$-\frac{1}{3}\left(\frac{E}{N}\right)^2 u \frac{df}{du}[Q_m]^{-1} = \int_{u_j}^{u+u_j} Q_j(u)\,f(u)\,du$$

which, in a gas mixture, becomes

$$-\frac{1}{3}\left(\frac{E}{N}\right)^2 u \frac{df}{du}\left(\sum_i \delta_i Q_{mi}\right)^{-1} = \sum_{ij} \delta_j \int_u^{u+u_j} Q_j(u)u\,f(u)\,du$$

where δ_j is the fractional concentration of the jth neutral species N_j/N.

Shown in figures are electron energy distribution functions f(u) calculated for various E/N values for CO_2 - N_2 - He mixture ratios 1-1-8 and 1-2-3. The function f(u) is normalized by:

$$\int_0^\infty \sqrt{u}\ f(u)\ du = 1$$

A reduced average energy u_r defined by Nighan as

$$\bar{u}_r = \frac{2}{3} \int_0^\infty u^{1/3}\ f(u)\ du$$

gives a value representative of the mean electron energy.

B/ - ELECTRON FRACTIONAL POWER TRANSFER

Once the distribution function f(u) for a given E/N is known the drift velocity v_d is given by

$$V_d = -\frac{1}{3}\sqrt{\frac{2e}{m}}\ \frac{E}{N} \int_0^\infty u \frac{df}{du}\ [Q_m]^{-1}\ du$$

from which

$$e\ V_d\ E/N = \sum_{j,i} \delta_j\ u_j \cdot \frac{\bar{\theta}_j D_R}{N_j}$$

where the collision frequency $\bar{\partial}_j D_R/N_j$ is defined by:

$$\bar{\delta}_j D_R/N_j = \sqrt{\frac{2e}{m}} \int_0^\infty u\ f(u)\ Q_j D_R(u)\ du$$

The total electric power density put into the discharge is obtained

$$jE = e\ N_e\ V_d\ E = N_e N \sum_{j,i} eu_j \frac{Q_{ji}}{N_j}$$

j being the electron current density.

If u_{j1} is the energy required to excite the first vibrational level, the effective collision frequency may be expressed:

$$\partial_{eff/N_j} = \sum_{D_R} \frac{u_j D_R}{u_{j1}} \frac{\bar{\partial}_j D_R}{N_j} \qquad \frac{\theta_{eff}}{N_1} = \sum_i \frac{u_i}{u_1} \frac{\theta_{ij}}{N_1}$$

The total power fed to the vibrational mode of the i-th molecule is:

$$\partial_{eff/N_j}\ u_{j1}\ N_j\ Ne$$

The effective collision frequency is sensibly independent of gas mixture when it is expressed as a function of the reduced average energy $\bar{u}_r$.

The fraction power transfer is obtained by dividing each term by the total power density j E. Figures show the percentage of power fed to the various vibrational and electronic levels N_2 and CO_2. For E/N of about 2.10^{-16} V.cm^2, for mixture of $CO_2 : N_2 : He = 1 : 2 : 3$, about 80% of the electron energy goes directily to the CO_2 upper laser level (001) and the first eight vibrational levels of N_2.

The discharge power density may be written in the form:

$$jE = \left(\frac{Ne}{N} e \nu_d \frac{E}{N} \right) N^2$$

In developing high power high efficiency molecular lasers, the discharge power density is as also significant as the vibrational excitation efficiency. To a first approximation, the discharge power density varies nearly as the square of the neutral gas density. The fractional ionization is generally about 10^{-7} - 5.10^{-8}, while the E/N ratio, once the mixture is specified, is nearly constant as also v_d which is approximately proportional to E/N.

D/ - POPULATION INVERSION AND GAIN

The fractional electron power transfer to the CO_2 (ν_3) and N_2 vibrational modes must be interpreted as the fraction of the fraction of the electric power that is potentially available for conversion to optical energy.

Increasing vibrational temperature leads to substantial increased gain at low vibrational temperature which corresponds to a low average number of quanta per molecula, tipically 0.1 for T_v – 1500 K. At higher vibrational temperature, the gain increases very slowly because the 001 population reaches a maximum for T_v about 4600 K for which to mean number of quanta per molecule is then about unity. A constant gas temperature, the mean number of vibrational quanta in the $_3$ mode is

nearly proportional to the electron density. Hence, a factor increase of about 10 in the electron density is needed to increase the vibrational temperature from 1500 to 4600 K.

II - CW electrically excited CO_2 lasers

In recent molecular lasers, the energy in excess deposited in the gas is removed convectively by flowing the gas mixture through the discharge region at high subsonic speed or even, in some cases, at supersonic speed.

The effect of the flow speed on the vibrational and translational energy equation may be seen from the expression:

$$jE = W_{el} = \rho u^2 \frac{du}{dx} + C^{M}_{p} \frac{\rho u}{M} \frac{dT}{dx} + \frac{\rho u}{M} \frac{dE_{vib}}{dx}$$

where u is the flow velocity, p is the gas density, M the molecular M weight, Cp the molecular specific heat, T the translational temperature and E_{vib} the vibrational energy per mole of gas mixture. Assuming that the velocity is nearly constant,

$$jE = \frac{\rho u}{M} \left(C^{M}_{p} \frac{dT}{dx} + \frac{dE_{vib}}{dx} \right)$$

The relaxation equation for the mean number of quanta per molecule is:

$$\frac{dA}{dx} = -\frac{A-A^e}{ru} + \frac{Rp}{u} \quad , \quad E_{vib} = R\Theta A$$

where r is the V-T relaxation time. Ae is the equilibrium value of A, i.e. for Tv = T and Rp = eff/N_jNe is the pumping rate.

6. E-beam assisted ionization

High power molecular lasers must operate at power densities below those imposed by thermal limitations. These plasma instabilities result in a non uniform discharge. Enhancement of discharge stability may be achieved by using an external control of the electron density. Electron beam sustained laser discharge in which ionization is provided uniformly through the laser volume with a high energy (~ 100 keV) electron beam is considerable interest.

In self-sustained discharges, the ionization process is dominated by direct impact ionization of the molecules. Only electrons in the high energy portion of the electron distribution, in the range 10-20 eV partecipate in this process.

On the other hand, it is seen that a small disturbance in E/N and therefore in the reduced energy $\bar{u}r$ leads to large fluctuations in electron density which has a dominant influence on discharge stability.

In e-beam sustained discharges, the applied field or drift field does not sustain the plasma as in self-sustained discharge do that E/N can be independently adjusted to optimize vibrational excitation of the upper laser levels.

The average energy E_s deposited per primary electron over the path z_1 to z_2 in the gas of constant density p is given by:

$$E_s = \frac{p}{z_2 - z_1} \int_{z_1}^{z_2} \frac{dE}{dz}\, dz$$

The electron-ion pair production rate in the gas is:

$$S_e = n_i \frac{J_{eb}}{e} \frac{E_s}{E_{ion}}$$

where n_i is the fraction of dissipated energy used in the ionization, J_{eb} is the electron beam current density, e is the electron charge and E_{ion} the average ionization potential of the gas mixture. In large volume-high pressure molecular lasers, the electron density Ne is controlled by the two-body recombination coefficient α_r or by the attachment coefficient α. The time dependent electron density is:

$$\frac{dNe}{dt} = - \alpha_r N_i N_e + S_e$$

where the ion density N_i is equal to N_e if negative ion concentration is very low. The steady-state electron density is:

$$Ne = \sqrt{\frac{S_e}{\alpha_r}} = \sqrt{\frac{n_i}{\alpha_r} \frac{J_{eb}}{e} \frac{E_s}{E_{ion}}}$$

The drift current density $J_d = e\, N_e\, V_d$ is easily obtained when the drift velocity has been calculated from Eq.5.

The drift power density in the plasma caused by the drift field E_d is $J_d\, E_d$ and for a constant E_d/N value, it is proportional to $N^{3/2} J_{eb}^{1/2}$ where N is the gas density.

References

1. A Maitland and M.H. Dunn, "Laser Physics", North Holland (1969).

2. D.C. Sinclair and W.E. Bell, "Gas Laser Technology", Holt, Rinehart and Winston (1969).

3. C.K.N. Patel, "Gas Lasers", in Lasers, a Series of Advances, Vol.2, Ed. A.K. Levine, pp.1-190, Dekker, 1988.

4. C.K.N Patel, "Vibrational-Rotational Laser Action in Carbon Monoxide" Phys. Rev. 141, 71 (1966).

5. R.L. Taylor and S. Bitterman, "Survay of Vibrational Relaxation Data for Processes Important in CO_2-N_2 Laser System", Rev. Modern Physics, 41, 26 (1969).

6. K. Smith, R. Thomson, "Computer modeling of gas lasers", Plenum Press (N.Y. 1978).

7. R. Bruzzese, S. Solimeno, G. L. Braglia, S. Martellucci, Ionic and thermal instabilities in e-beam preionized CO_2 EDCL devices in the presence of a laser beam, Il Nuovo Cimento 60B, 113 (1980)

8. S. Solimeno, S. Martellucci, High power chemical lasers in "Developments in high power lasers" (1981).

9. L.S. Frost and A.V. Phelps, Phys. Rev 127, 1621 (1962)

10. Willet, "Gas lasers", Pergamon Press

11. Witteman, CO_2 lasers, Springer Verlag (1987)

12. G. Herzberg, "Molecular Spectra and Molecular Structure", vol. 2, Van Nostrand, N.Y. (1945).

13. R.J. Harrach and T.H. Einwolmer, "Four-Temperature Kinetic Model for a CO_2 Laser Amplifier", Lawrence-Livermore Laboratory, Livermore UCRL-51399 May 1973

14. M. Gross and A.N. Chester, "Chemical Lasers" J. Wiley

15. W.L. Nighan, Phys. Rev. A2, 1989 (1970)

16. W.L. Nighan and W.J. Wiegand, Phys. Rev. A10, 922 (1974)

17. R.A. Haas, Phys. Rev. A8, 1017 (1973)

18. A. L. Bloom, "Gas Lasers", J. Willy and Sons, N.Y. (1968)

19. C. A. Fentermacher, M. I. Nutter, W.T. Leland, and K. Boyer, Appl. Phys. Lett. 20, 56 (1972)

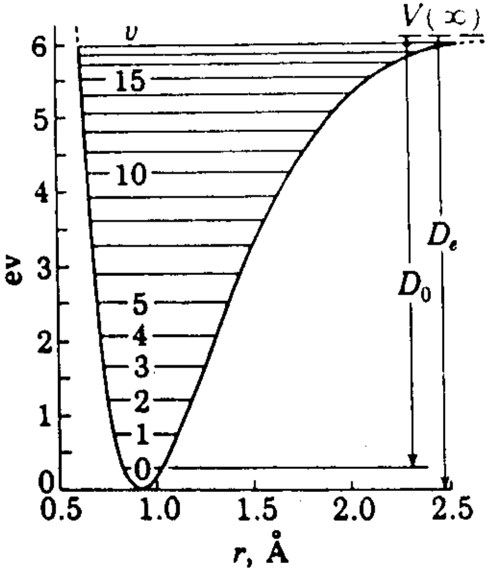

Potential energy curve and vibrational levels for the ground state of hydrogen fluoride

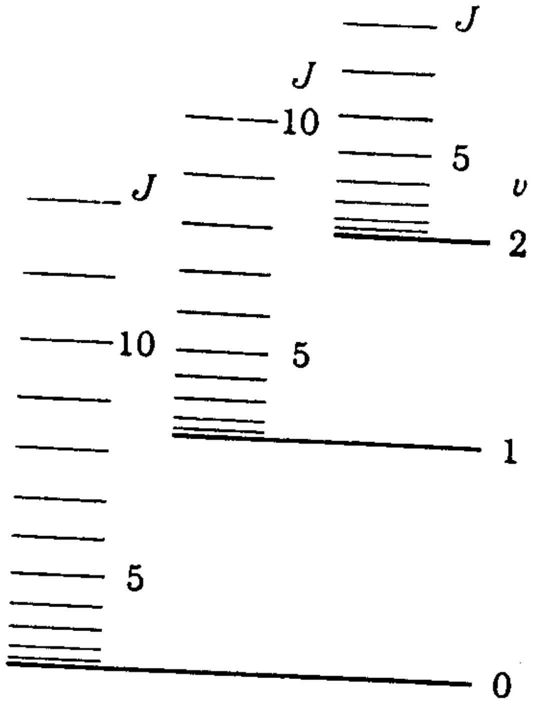

Vibrational and rotational levels for a diatomic molecule

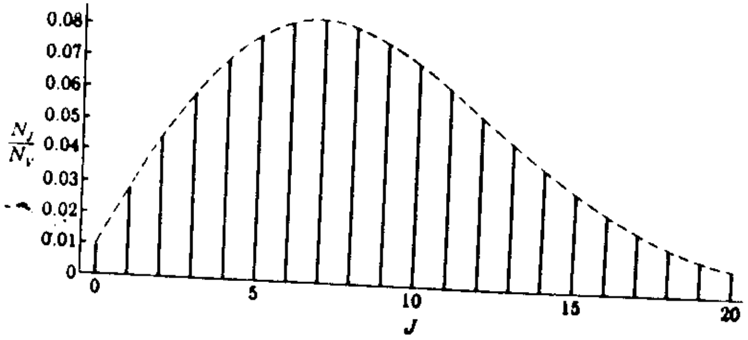

Relative populations of rotational levels in the v = 0 state of the ground electronic state of CO $T = 300^{\circ}K$, $B_o = 1.9225\ cm^{-1}$

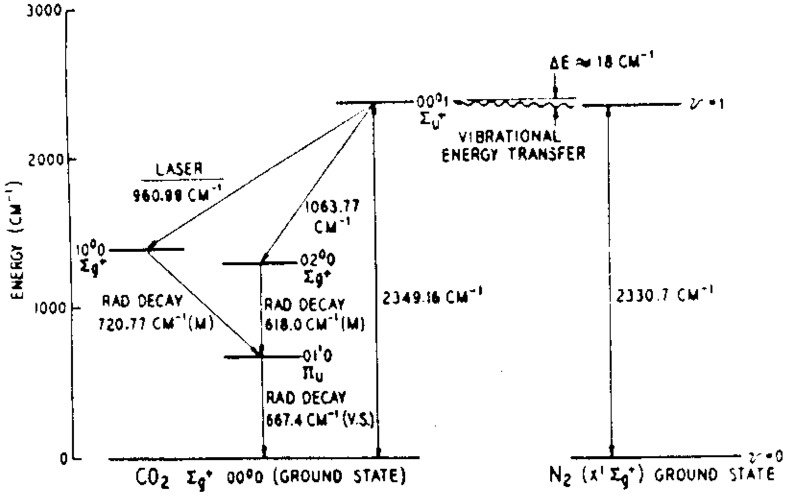

Energy level diagram of N_2 and CO_2

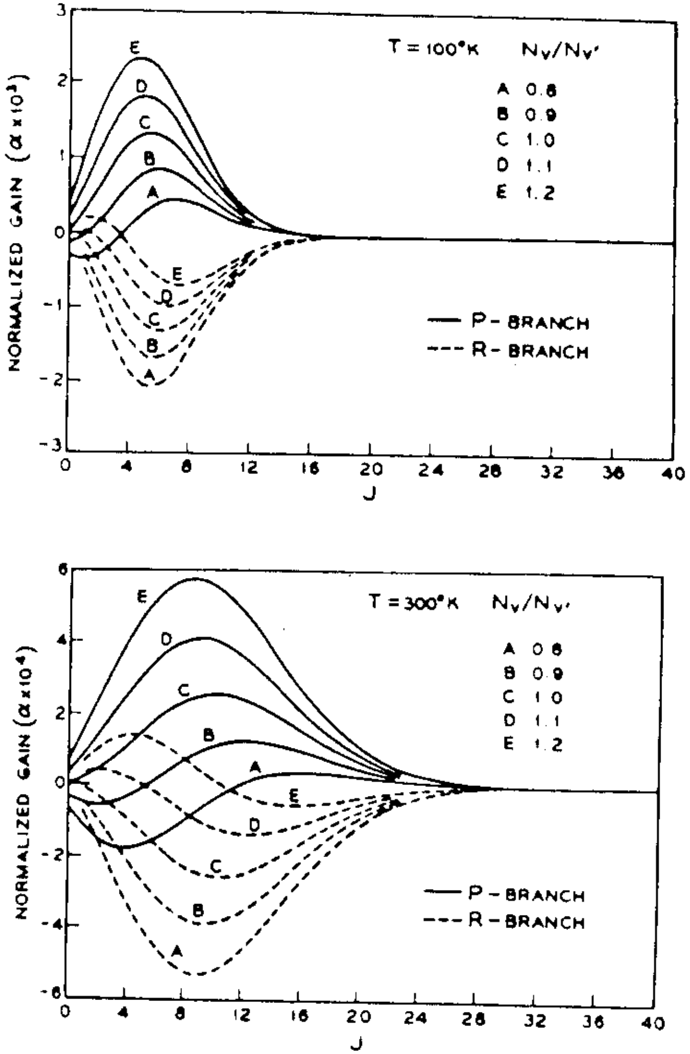

Normalised gain for 7-6 vibration-rotation band of CO plotted as a function of upper level J

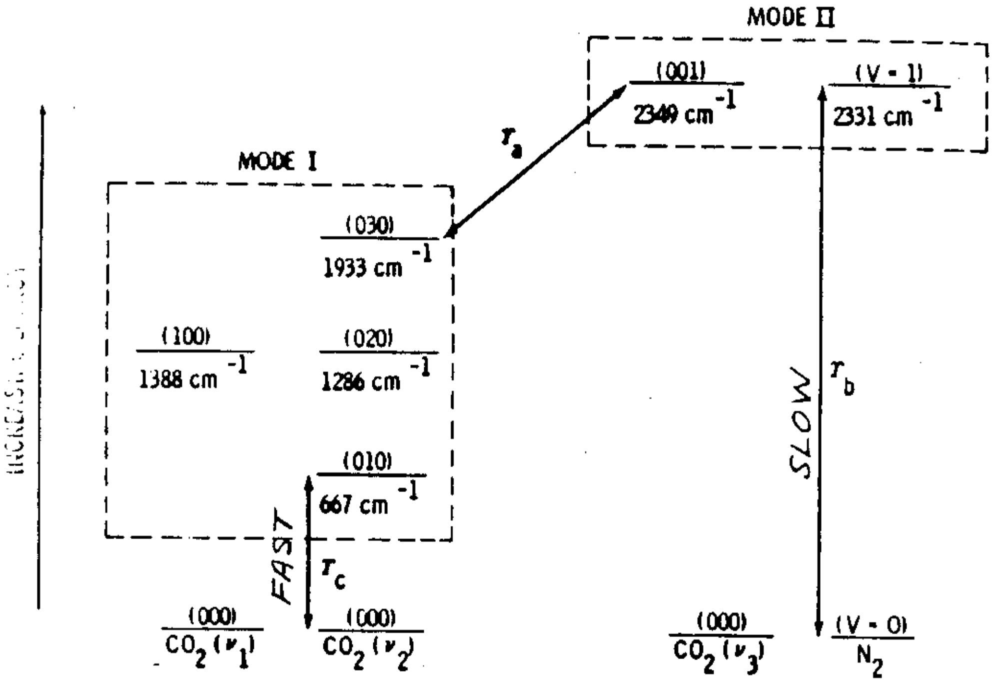

Schematic of the grouping of energy levels for the vibrational model

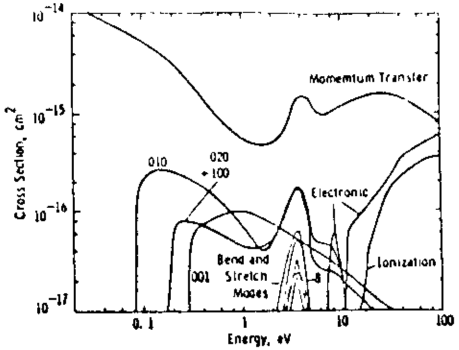

Cross section for momentum transfer and inelastic scattering for electrons in CO$_2$

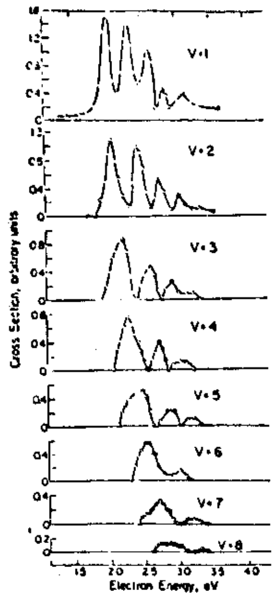

Cross sections for vibrational excitation of N$_2$

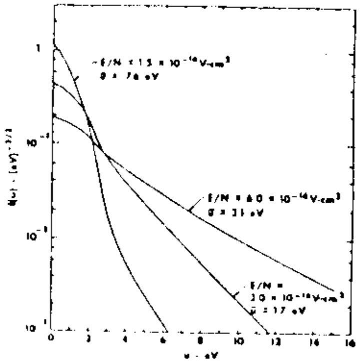

Electron energy distribution in CO_2 - N_2 - He mixture

1. Introduction

Scaling relationships of the gain as a function of the laser medium has suggested the use of waveguide systems in alternative to free space propagation in order to build compact high efficiency gas lasers (see fig. (1)). This concept was first proposed by Marcatili (1) who emphasized the possibility of getting HeNe laser operation taking advantage of the increase of laser gain with decreasing diameters (2). The first waveguide gas laser operation was achieved by Smith (3) who contructed an HeNe laser in a 20 cm long capillary tube with a 430 µm diameter. Successively many groups (4-7) have improved the theory and designed new kind of resonators. Their main advantages are small size, low weight, low cost and high efficiency. New capabilities will be features such as high pressure operation for tunability and mode control, longer lifetime, low operation voltages for TEA devices, transverse mode control, compatibility with waveguiding modulator structures, high gain and power per unit volume.

In particular, the CO_2 waveguide laser has been chosen for its tunability in spectroscopic and communications applications, and it is anticipated that miniature TEA lasers and waveguide FIR lasers will be used in applications where their properties offer many advantages.

In this section we shall briefly review the basic properties of a waveguide gas laser (WGL) describing the main features of some particular systems together with some typical applications.

1. The resonator problem

With reference to fig. 1 WGL basically consists of a hollow dielectric tube with arbitrary cross section and two external mirrors. WGL modes consist of a fiels distribution propagating inside the waveguide and radiating at its termination toward one mirror. The back reflected radiation is then coupled again inside the guide. The field distribution must, of course, reproduce itself after each round trip.

An exact analysis of this kind of resonators is very involved and many different approaches have been proposed. One is to compute the field distributions for a given resonator configuration iteratively for a large number of round trips through the cavity. Steady-state solutions develop after many passes which represent the eigenmodes of the resonator. This technique was developed for waveguide laser resonators by Chester and Abrams (4). A second approach is to develop a formulation describing a round trip through the cavity where the field distribution is expressed in terms of an expansion into a finite number of waveguide modes and a propagation matrix derived. Diagonalization of this matrix permits the calculation of the eigen modes and of their losses (8,9).

Before going on we must spend a few worlds on the modes of a hollow waveguide (1). The modes of hollow dielectric waveguides differ in nature from the modes of conventional fiber optical waveguide. Conventional dielectric waveguide modes are guided by total internal reflection of optical rays at a dielectric interface: the rays propagate through a core region having a refractive index higher than the surrounding medium. In a hollow waveguide the guiding (or core) region has a lower refractive index than the surrounding media and waveguiding takes place owing to nearly total internal reflection at the dielectric interface (total internal reflection is not possible). Some radiation inevitably leaks into the dielectric medium and radiates. For this reason the modes are often referred to as leaky modes and this results in a finite waveguiding loss, even allowing perfect geometry and no material absorption. This loss is strongly dependent on waveguide dimensions and limits operation of hollow waveguides to highly overmoded structures.

The circular guide supports three basic types of modes: transverse circular electric, whose electric field is to first order tangential to the waveguide surface; transverse circular magnetic, whose magnetic field is to first order tangential to the waveguide surface and whose electric field is radial; and hybrid modes which have both tangential and radial electric and magnetic fields (Fig. 2). The field distributions are considerably simplified if we assume

$$ka \gg |v| u_{nm}$$

where $k=2\pi/$ is the free space propagation constant, v is the complex refractive index of the dielectric wall, u_{nm} is the mth root of $J_{n-1}(u_{nm})=0$ and n,m are integers labeling the mode.

The lowest-order hybrid mode, EH_{11}, is linearly polarized and closely resembles a TEM_{00} gaussian mode. The propagation constant for the various modes is given by (1)

$$\gamma_{nm} = k\left[1 - \frac{1}{2}\left(\frac{u_{nm}}{2\pi a}\right)^2\left(1 - \frac{i v_n}{\pi a}\right)\right] = \beta_{nm} + i\alpha_{nm}$$

where the constant v_n depends on the type of mode being considered and the refractive index of the guide wall.

$$v_n = \begin{cases} \dfrac{1}{(v^2 - 1)^{½}} & \text{for } TE_{0m} \text{ modes} \\ \dfrac{v^2}{(v^2 - 1)^{½}} & \text{for } TM_{0m} \text{ modes} \\ \dfrac{\frac{1}{2}(v^2 + 1)}{(v^2 - 1)^{½}} & \text{for } EH_{nm} \text{ modes} \end{cases}$$

As previously pointed out the mode analysis in a WGL is very difficult and a complete review of the different approaches would be rather long and beyond the aim of these notes. Therefore, here we limit to calculate only the coupling losses of a given mode between the guide and the mirror referring to specific literature for a more complete and detailed analysis.

To this end, we consider a hollow dielectric waveguide terminated by flat mirrors normal to the guide axis at the ends of the guide. A mode in the guide is reflected back on itself at the end points and suffers no coupling loss. Thus, the modes of the resonator consist of the usual set of longitudinal modes and, since different waveguide modes have different propagation constants, they are associated with transverse modes or field distributions given by the hollow waveguide modes. The losses of these modes are then simply the losses associated with propagation in the leaky waveguide. If the mirrors are then moved away from the end of the guide, which is the usual laser condition, the modes will suffer additional losses because of imperfect coupling of the radiation back into the guide after propagating to the mirror and back. In this section we calculate these coupling losses as functions of mirror position and mirror radius for EH_{11} lowest-order linearly polarized mode. In solving the radiation problem at the end of the guide, we will decompose the field amplitude into free space gaussian normal modes.

2. Waveguide gas lasers

As the mirrors are moved away from the end of the guide, increasing coupling losses occur as a result of two effects: (1) the field may not reenter the guiding structure; (2) some of the energy is converted to higher-order waveguide modes. To the extent that the second condition occurs, the modes are not truly pure modes and the problem we are really solving is that of a single-mode EH_{11} mode filter in place of a multimode waveguide. However, we shall see that the EH_{11} waveguide mode couples 98% of its energy to the TEM_{00} lowest-ordergaussian free space mode for optimum choice of gaussian beam parameters.

First we choose our expansion functions as Gaussian-Laguerre normalized modes(10)

$$\Psi_p = \frac{2}{\sqrt{\pi}} \frac{1}{w_o} L_p\left(\frac{2r^2}{w_o^2}\right) \exp(-r^2/w_o^2)$$

where L_p is the Laguerre polynomial of degree p, and w_o the 1/e radius of the mode amplitude.

The first consideration for choosing a set of modes is to decide what value to take for w_o. Clearly, since we have a complete set of expansion functions, any value is suitable for solving the radiation problem, but some values are more physically meaningful than others and should lead to a more rapidly converging series.

Taking the lowest-order waveguide mode as $E(r)=J_o(ur/a)$, the expansion coefficients are given by ($u=u_{11}=2.405$ for theEH_{11} mode).

$$A_p = \sqrt{\frac{2}{\pi}}\,\frac{1}{w_o}\int_0^a J_o\left(\frac{u}{a}r\right) L_p\left(\frac{2r^2}{w_o^2}\right)\exp(-r^2/w_o^2)\,2\pi r\,dr$$

$$= \sqrt{\frac{\pi}{2}}\,w_o\int_0^k J_o(\sqrt{x})\,L_p(x)\,\exp(-x/2)\,dx,$$

$$= \sqrt{\frac{u}{2}}\;\frac{w_o}{a}, \qquad K = 2a^2/w_o^2.$$

A_o is maximized for $w_o/a = 0.6435$ (a being the radius of the guide). For this value of w_o/a 98% of the energy contained in the incident gaussian mode is coupled into the fundamental mode of the guide. Therefore, hereafter, we shall refer to this value of w_o/a.

With reference to fig. 3 the simplest way to calculate the coupling losses consists of propagating the field at the output of the guide down to the mirror and calculating the projection of the resulting field on EH_{11} mode. Figure 4 shows the coupling losses as a function of R/Z_R and Z/Z_R $Z_R=\pi w_o^2/$ being the Rayleigh length (5).

The calculation of the coupling losses is far from being exhaustive. The complete mode analysis can be carried out by taking advantage on two different approaches: iterative technique and matrix formulation.

The iterative technique is quite similar to the algorithm developed by Fox and Li (11) to analyze open resonators. Following this procedure Chester et al. (12) analyzed the simplified WGL shown in fig.5. In particular a numerical simulation of the experiment performed by Smith (9,13,14) was carried out. The following numerical values were assumed: λ =6328 Å, a=200 µm, L=20cm, R=30cm. With these values Chester (12) obtained the results plotted in fig. 6.

Degnan and Hall (9) presented a theory for waveguide resonators which reduced the calculation to the diagonalization of a complex matrix. They treated the radiation in the free space region from the guide to the mirror by a Fresnel-Kirchoff diffraction integral, took account of finite mirror aperture and curvature, and then performed a second integration for calculating the return wave to the waveguide aperture.

This technique can be notably simplified if mirrors of infinite aperture are assumed (4).

In the matrix formulation(9) the electromagnetic field in the wave guide is represented by an expansion over an arbitrarily large set of waveguide modes. The coefficients of the expansion form the components of a column vector describing the mode, which is then easily propagated through the waveguide using the known propagation constants for the various modes. At the end of the guide, the electromagnetic field is numerically evaluated via a transformation matrix onto a finite mesh. The radiation is propagated through the equivalent lens and back onto the waveguide via a Fresnel-Kirchoff diffraction integral, where it is then expanded into waveguide modes via the inverse of the above transformation matrix. This process is repeated until one complete round trip is made through the resonator. Multiplying all the steps together results in a M x M complex propagation matrix for the waveguide resonator, where M is the initial number of modes used in the expansion. The matrix is then numerically diagonalized. The resulting eigenvectors represent the transverse modes of the resonator, and the eigenvalues yield the corresponding mode losses and the phase shifts experienced by each mode relative to free space propagation.

With reference to fig. 1, fig. 7 shows some numerical results obtained by the matrix formulation for a symmetric resonator $Z_1=Z_2=Z=Z_R$ $R_1=R_2=R=2Z_R$.

The use of optical waveguiding allows one to extend the operation of gas lasers to smaller diameter discharges without being limited by the usual diffraction losses incurred in free space propagation. In this section we discuss the plasma scaling relationships which allow us to predict how laser parameters such as gain, efficiency and power output will change with decreasing discharge diameter. While these relationships can be used as guidelines to anticipate useful operating ranges of various laser systems, the precise dependence of laser parameters on discharge diameter will be only determined by experiment (2,15,16).

Given that optimum conditions have been determined for a particular tube geometry, the table tells us that as the tube diameter is made smaller:

the pressure increases,
the current decreases,
the voltage increases,
the gain increases,
the power per unit length remains the same,
the efficiency remains the same.

3. CO_2 Waveguide lasers

Application of the waveguide laser principle to the CO_2 laser system was first accomplished by Bridges et al. (17) using flowing gas mixtures of CO_2-He-N_2 in a 1 mm diameter x 30 cm long glass capillary tube. They observed substantial increases in gain, output power per unit volume and saturation intensity over conventional CO_2 laser devices.

Burkhardt (18) showed improved operating characteristics in 1 mm diameter x 10 cm long BeO ceramic tubes. Power output up to 2.4 W and gain coefficients as high as 27 dB/m were realized at high flow rates.

Motivated by the need for tunable sealed-off lasers in CO_2 laser communications systems, Abrams (4) described the performance characteristics of sealed-off CO_2 waveguide laser devices. The emphasis was on high pressure operation (300 Torr) where collision broadening of the CO_2 laser transition exceeds 1 GHz. The particular need was a Doppler tracking laser local oscillator for a heterodyne receiver.

For mixtures rich in CO_2 the gain peaks at low pressure, while for mixtures lean in CO_2 the peak gain is lower but peaks at higher pressure. It is clear that significant output can be achieved at pressures in excess of 200 torr.

Small amounts of N_2 and Xe were added to selected He-CO_2 mixtures. In general, it was found that ½ part N_2 and ¼ part Xe give optimum gain, but only resulting in a 10% increase over the He-CO_2 data.

Now, we briefly describe some particular CO_2 waveguide laser systems. The limited tuning range of conventional Doppler-broadened CO_2 lasers (53 MHz) has limited their utility in laser communications, optical radar, pollution detection and spectroscopy. Operation of waveguide CO_2 lasers at high pressure can result in pressure broadening of the laser transition and much larger available gain bandwidth for frequency tuning and other applications.

The tunable laser, shown in fig. 8, was fabricated from four polished BeO slabs, 9.5 cm long, epoxied together to form a 1.0 mm square waveguide. Copper gasketed vacuum flanges are machined to fit over the rectangular outer dimensions of the tube, and are epoxied to the ceramic. Laser output is taken off the zeroth order from the 150 l/mm diffraction grating used in the Littrow configuration for line selection.

This laser was used by Abrams (19) to directly measure line shapes and pressure broadening coefficients for the CO_2 laser transition. A similar tunable waveguide CO_2 laser has been incorporated into a Doppler tracking heterodyne communications system built for NASA by Goodwin (20) and a flowing gas version of the laser was used by Menzies and Shumate (21) in airborne heterodyne ozone monitoring experiments.

Modulation of CO_2 laser radiation for wideband communications has best been achieved by coupling modulation. In this scheme, an electro-optic CdTe crystal is placed within the laser cavity where the circulating optical power far exceeds the laser output power. Application of modulating voltage to the modulator results in polarization modulation of the circulating power which can be coupled from the cavity. Using this technique, Kiefer et al. (22) demonstrated efficient coupling modulation with bandwidhts in excess of 200 MHz.

Goodwin et al. (20) have extended this concept to waveguide CO_2 lasers. Waveguide lasers are ideally suited for intracavity coupling modulation owing to the fact that a guided mode within a square cross-sectioned hollow waveguide can couple very efficiently into an electro-optic modulator rod of the same cross section. A sheme of the sealed-off laser transmitter developed for NASA is shown in fig. 9.

A number of CO_2 laser applications demand for pulsed output. The requirements vary far from the relatively low pulse rates and high energy per pulse required for laser rangefinders and designators to the very short pulse rates required for laser communications. Many of the techniques that have been used for producing pulsed output with conventional CO_2 lasers have been applied to waveguide CO_2 lasers. They include mode locking, Q-switching and gain switching.

Mode locking of waveguide CO_2 lasers is an attractive possibility because the large pressure-broadened linewidth allows for generation of very

short pulse widths. Smith et al. (13) first demonstrated mode locking of a waveguide CO_2 laser with flowing gas. They produced a cw train of 3 ns wide pulses via intracavity loss modulation at the C/2L frequency using germanium intracavity acousto-optic modulator.

4. Noble gases

Smith (3) built the first visible wavelength waveguide laser, a He-Ne laser operating at 6328 A. The primary feature of the waveguide He-Ne laser are:

(1) Higher gain due to the inverse dependence of gain on discharge diameter.

(2) Higher operating pressure (~ 7 torr) resulting in nearly homogeneous broadening of the He-Ne laser transition. This causes the laser to operate in the highly desired single mode condition owing to strong mode competition effects.

(3) Excellent transverse mode control is achieved via the unique properties of waveguide resonators.

Smith and Maloney (13) demonstrated some unique features of the He-Xe laser system at 3.5 µm operated in the waveguide geometry. This transition exhibited extraordinary gain coefficients, approaching 1000 dB/m in a 250 µm bore. Single isotope He^3-Xe^3 was used with a combination of dc and rf excitation. An amazing property of such high gain lasers is the strong dispersion associated with the gain, resulting in pronunced mode pulling effects.

All the molecular lasers which had been successfully operated in conventional resonators should be operable in the waveguide configuration.

The electrically excited CO laser is a good candidate because of its high efficiency and cw operation. Yusek and Lockhart (23) obtained cw operation in sealed-off glass capillaries at a wall temperature of 250 °K. They achieved 300 mW output from a 2 mm diameter discharge at an optimum operating pressure of 65 torr.

Asawa (24) reported measurements on a 2 mm dia x 14 cm long sealed-off BeO tube cooled by dry ice to 250 K. He achieved 1.1 W output at 5.7% efficiency in a single mode. Optimum pressure was found to be 80 torr (close to the value reported above) with a CO-He-Xe-N_2 mixture of 1:8:1:1.

Evidence that the waveguide laser principle is quite general was given by Bua and Rudko (25). Operation of miniature waveguide TEA lasers with a number of molecular and atomic gases in the near infrared was demonstrated. Lasing was accomplished in HF(2.8μm), DF(3.8μm), HBr(4.2μm), CH_3I(3.04μm), ArF(1.69μm), Xe(2.03μm) and Ar(1.25, 1.28μm). They found that output power and efficiency increase with anode to cathode distance.

References

1. E.A.J. Marcatili, R.A. Schmeltzer, Bell Syst. Tech. J., 43, 1783 (1964)
2. E.I. Gordon, A.D. White, Appl. Phys. Letters, 3, 199 (1963).
3. P.W. Smith, Appl. Phys. Letters, 19, 132 (1971).
4. R.L. Abrams, A.N. Chester, Spring Meeting of Optical Society of America, Denver, CO, paper ThD16 (1973).
5. R.L. Abrams, IEEE J. Quantum Electronics, QE-8, 838 (1972).
6. J.J. Degnan, Appl. Optics, 12, 1026 (1973).
7. F.K. Kneubuhl, J. Opt. Soc. Amer., 67, 959 (1977).
8. R.L. Abrams, Appl. Phys. Letters, 25, 304 (1974a).
9. J.J. Degnan, D.R. Hall, IEEE International Electron Devices Meeting, Washington, D.C. (1972).
10. H. Kogelnik, T. Li, Appl. Optics, 5, 1550 (1966).
11. A.G. Fox, T. Li, Bell Syst. Tech. J., 40, 453 (1961).
12. A.N. Chester, R.L. Abrams, Appl. Phys. Letters, 21, 576 (1972).
13. P.W. Smith, P.J. Maloney, Appl. Phys. Letters, 17, 259 (1973).
14. P.W. Smith, T.J. Bridges, E.G. Burkhardt, O.R. Wood, Appl. Phys. Letters, 21, 470 (1973a).
15. V.K. Konyukhov, Sov. Phys. J. Tech.Phys., 15, 1283 (1971).

16. G. Francis, Handbuch Der Physik, Glow Discharge at Low Pressure (Springer-Verlag; Berlin), 53-195 (1956).

17. T.J. Bridges, E.G. Burkhardt, P.W. Smith, Appl. Phys. Letters, 20, 403 (1972).

18. E.G. Burkhardt, T.J. Bridges, P.W. Smith, Opt. Commun., 6, 193 (1972).

19. R.L. Abrams, Appl. Phys. Letters, 25, 609 (1974b).

20. F.E. Goodwin, Opto-Mechanical Sybsystem of a 10 µm Wavelength Receiver Terminal, National Aeronautics and Space Administration Contract NAS 5-21859 (1975).

21. R.T. Menzies, M.S. Shumate, IEEE/OSA Conference on Laser Engineering and Applications, Washington, D.C., paper 15.10 (1977).

22. J.E. Kiefer, T.A. Nussmeier, F.E. Goodwin, IEEE J. Quantum Electronics, QE-8, 173 (1972).

23. R. Yusek, G. Lockhart, IEEE/OSA Conference on Laser Engineering and Applications, Washington, D.C., paper 16.1 (1973).

24. C.K. Asawa, Appl. Phys. Letters, 24, 121 (1974).

25. D.P. Bua, R.I. Rudko, IEEE/OSA Conference on Laser Engineering and Applications, Washington, D.C., paper 6.9 (1977).

26. M. Inguscio, N. Ioli, G. Moruzzi, F. Srumia, Opt. Comm. 37, 211 (1981).

27. S. Solimeno, in "Workshop on laser acceleration of Particles", AIP-92 Los Alamos (Feb. 1982).

28. A. Cutolo, S. Solimeno, Opt. Comm. 43, 323 (1982).

Table

Quantity	Relation
Gas number density N	$D_2N_2 = N_1D_1$
Gas pressure p	$p_2D_2 = p_1D_1$
Electron temperature T_e	$T_{e2} = T_{e1}$
Electron density N_e	$N_{e2}D_2 = N_{e1}D_1$
Current Density J	$J_2D_2 = J_1D_1$
Current I	$I_2/D_2 = I_1/D_1$
Electric field E	$E_2D_2 = E_1D_1$
DC resistance Z	$Z_2D_2^2 = Z_1D_1^2$
Power input/length P_i/L	$P_{i2}/L = P_{i1}/L$
Gain coefficient α	$\alpha_2D_2 = \alpha_1D_1$
	$\alpha_2 = \alpha_1$
Saturation flux density S	$S_2D_2 = S_1D_1$
	$S_2D_2^2 = S_1D_1^2$
Power output/volume P_o/V	$(P_{o2}/V)D_2^2 = (P_{o1}/V)D_1^2$
Power output/length P_o/L	$P_{o2}/L = P_{o1}/L$

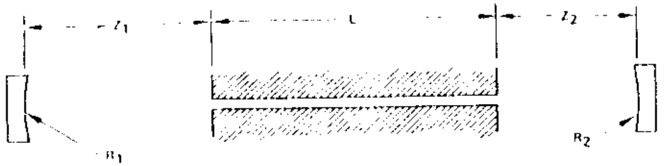

Fig. 1 Schematic of a hollow waveguide resonator.

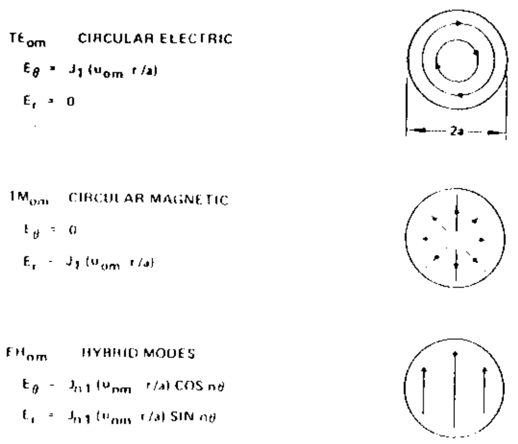

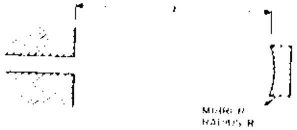

Fig. 3 Geometry for the calculation of the coupling losses.

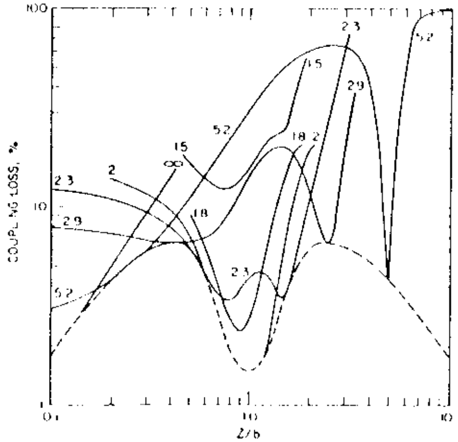

Fig. 4 Coupling loss versus mirror position for the case where the mirror radius matches the curvature of the wavefront (dashed line) and for mirrors of fixed curvature. Each curve is labeled with the value of R/Z_R.

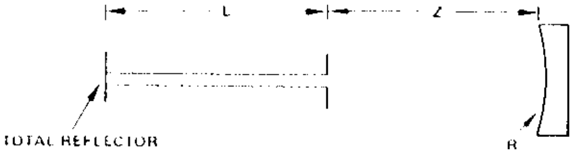

Fig. 5 Half symmetric waveguide resonator.

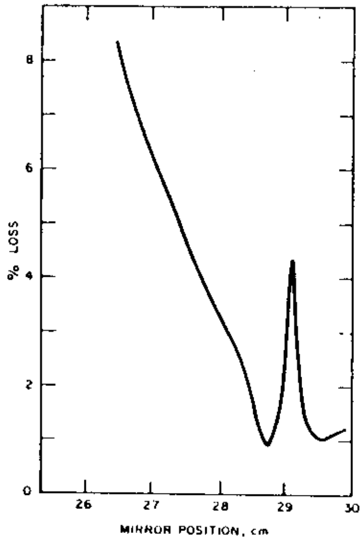

Fig. 6 Coupling losses for the WGL built by Smith (2).

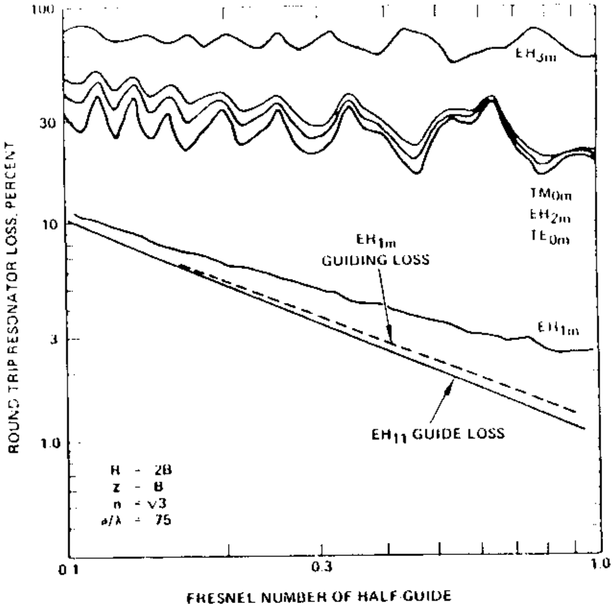

Fig. 7 Round-trip resonator loss versus Fresnel number of the half-guide for the lowest loss mode of each resonator mode class. The dashed line is the guiding loss of the EH_{1m} resonator mode. The guiding loss of the EH_{11} waveguide mode is shown for comparison. For these curves, $R=2B$, $Z=B$, $v=\sqrt{3}$ and $a/\lambda=75$ (Abrams and Chester 1974).

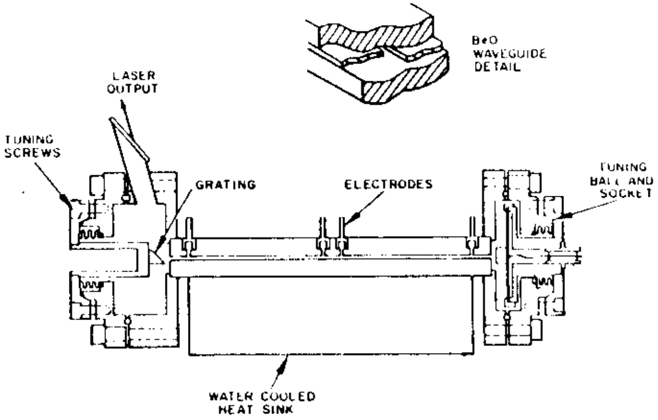

Fig. 8 Schematic of a tunable waveguide laser.

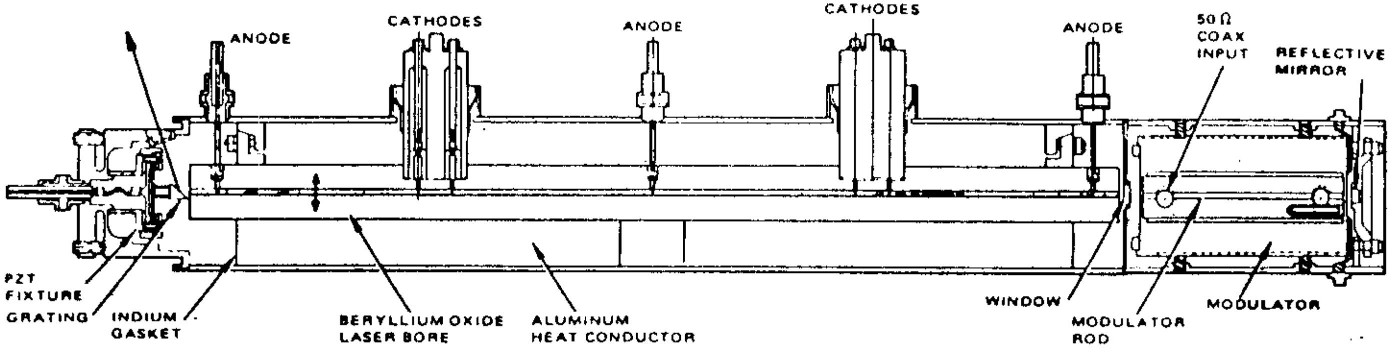

Fig. 9 Shematic of a waveguide laser transmitter constructed for NASA (20).